Springer

Journal of Mechanical Science and Technology 23 (2009) 1736~1742

Journal of Mechanical Science and Technology

www.springerlink.com/content/1738-494x
DOI 10.1007/s12206-009-0421-5

A study on the flow with nonequilibrium condensation in a minimum length nozzle †

Soon-Bum Kwon*, Sung-Jin Lee, Seung-Young Shin and Sung-Ha Kim

School of Mechanical Engineering, Kyungpook National University, 1370, Sankyuk-dong, Daegu 702-701-, Korea

(Manuscript Received January 22, 2009; Revised March 25, 2009; Accepted April 7, 2009)

Abstract

As recognized previously, a minimum-length nozzle has the smallest possible throat-to-exit length that is still capable of maintaining uniform supersonic flow at the nozzle exit. In the present study, for the flow of moist air through a nearly minimum-length nozzle designed by the method of characteristics, the effects of nonequilibrium condensation on the uniformity of flow properties, the momentum efflux, and the flow distortion at the nozzle exit plane are discussed by experiment and numerical analysis of a third-order Total Variation Diminishing (TVD) finite difference scheme. The onset and zone of nonequilibrium condensation in a minimum-length nozzle are quite different from those of a general convergent-divergent supersonic nozzle. We know that the uniformity of flow properties at the nozzle exit with regard to the flow with nonequilibrium condensation in a minimum-length nozzle cannot be guaranteed. On the other hand, owing to the positions of the onset of condensation at the incident region of expansion waves from the sharp corner just downstream of the nozzle throat, the deceleration gradient and magnitude of heat released from the process of nonequilibrium condensation to the surrounding of ϕ_0=60% are greater than those of ϕ_0=70% in the case of T_0=290K. Furthermore, it has been determined that the decrease in efflux of momentum from the nozzle exit for the stagnation relative humidity of ϕ_0=70%(T_0=290K), which corresponds to the case with nonequilibrium condensation shock, is 6.8% smaller than that of isentropic expansion.

Keywords: Flow distortion; Momentum efflux; MLN; Moist air; Nonequilibrium condensation; TVD scheme

1. Introduction

Since the initial observations related with nonequilibrium condensation made by Prandtl [1], many studies with respect to nonequilibrium condensation theories [2, 3] and to the supersonic flow with the nonequilibrium process of condensation have been conducted [4, 5]. The flow of nonequilibrium condensation can be found with regard to various engineering applications such as the flows of the steam turbine cascade, the expansion of moist air in a wind tunnel, and so on [6-8].

As is well known, it is essential that the flow exiting a wind tunnel nozzle (that is, the test section) be parallel and free of Mach waves at the desired exit Mach number. The presence of such waves is undesirable, because these waves can coalesce to form a shock wave and prevent the uniformity of flow in the test section. To properly cope with these harmful problems, it is recommended that a nozzle that is composed of expansion and straightening sections be designed. In fact, some nozzles such as minimum length nozzles (MLNs) or rapid expansion nozzle have no expansion section at all owing to the problems of weight and installing space, in which the initial expansion is created by a sharp corner at the nozzle throat. In general, minimum-length nozzles have been used in gas dynamic lasers and higher supersonic wind tunnels [9]. Despite the importance of the flow through a MLN, however, we could not find a

† This paper was recommended for publication in revised form by Associate Editor Do Hyung Lee

*Corresponding author. Tel.: +82 53 950 5578, Fax.: +82 53 950 6550
E-mail address: sbkwon@knu.ac.kr

study on the flow that intervenes with nonequilibrium condensation in MLNs. Thus, in the present study, the effects of nonequilibrium condensation on the uniformity of flow properties at the nozzle exit, the momentum efflux, the flow distortion of the entire flow field, and so on are reviewed by experimental and numerical analysis to cope with the problem caused by the latent heat released in the process of nonequilibrium condensation into the surrounding gas flow in a supersonic wind tunnel. Moist air is used as a working fluid. In our calculations, after initially confirming the validity of the adopted numerical method of the third-order TVD finite difference scheme, which is possible to compare the distribution of static pressure by experimenting with the result of numerical analysis on the centerline of the nozzle, the distribution of flow properties is calculated by using the verified TVD method. In our experiment, we used an intermittent indraft-type supersonic wind tunnel, in which the capacities with regard to the stagnation reservoir and sink tank are $40m^3$ and $5m^3$, respectively. To visualize the flow, we used a schlieren optical system with a light source of Xe of 1kw. Moist air was used as the working fluid.

2. Experimental facility and procedure

The intermittent indraft-type supersonic wind tunnel used in the present study is shown in Fig. 1. It mainly consists of a stagnation reservoir of $40m^3$, a sink tank of $5m^3$, a schlieren visualization optical system, and a pressure-measuring system consisting of a 16-channel scanning valve (model:DSA3017). Based on the flow field symmetry, this requires only one-half of the flow, that is, one-half of the nozzle system. In designing MLNs, we used a method based on the characteristics proposed by Hodge et al. [10] The design nozzle Mach number used in the present study is a constant value of 1.4. After the pressure in the sink tank has been kept below 0.2 kPa by a vacuum pump, by opening the vacuum valve installed downstream of the MLNs, the uniform flow of moist air from a circulation fan installed at the stagnation reservoir, expands to the pressure of the vacuum tank. In this case, the approximate duration time of 15s in a steady state at the nozzle exit can be sustained. The static pressures along the nozzle centerline are measured by a 16-channel scanning valve system in which the static hole measuring the static pressure is 0.8 mm in outer diameter. Owing to the possibility of

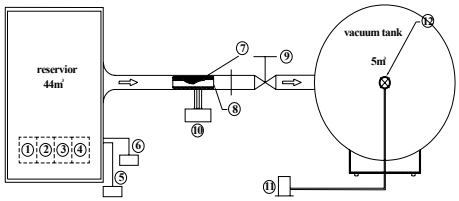

① HEATER	② AIR-CONDITIONER
③ WATER VAPOR GENERATOR	④ DEHUMIDIFIER
⑤ THERMOMETER	⑥ HUMIDITY INDICATOR
⑦ MINIMUM LENGTH NOZZLE	⑧ TEST SECTION
⑨ VACUUM VALVE	⑩ SCANNING VALVE
⑪ VACUUM PUMP	⑫ VALVE

Fig. 1. Schematics of the experimental apparatus.

nonequilibrium condensation at the approximate region designated as M=1.3, the static holes at the neighboring sites to this zone are densely packed.

The pressure sensed by the pressure transmitter (PTX-1400, Druck Co.) installed in the scanning valve system is A/D converted and then recorded by a personal computer. The pressure sensor error installed in the scanning valve is $\pm 0.05\%$ in full scale, and the scan rate is 200 samples per channel per second. The average value of measuring 3000 times at a measuring point of the bottom wall of the nozzle is decided as the static pressure at that point.

3. Numerical procedure

To analyze the two-dimensional steady-state supersonic flow with condensation, two-dimensional Navier-Stokes equations, in conjunction with a nucleation rate equation having a droplet growth equation, were used as numerical governing equations. In our calculations, we assumed that (1) the velocity difference between a droplet and its surrounding gas phase is negligible, (2) the liquid droplet in the flow field is distributed uniformly, (3) each component of the mixture is thermally and calorically perfect, (4) the droplets are extremely small such that there is no temperature gradient within the droplet, and (5) the thermal accommodation coefficient is 1 [11]. The equations of mass conservation, momentum, and energy related to the viscous adiabatic compressible flow of the mixture are given, and they are similar to their single-phase flows. The mathematical closure of these equations requires a separate equation for the wetness fraction, and this can be obtained based on the theo-

ries of condensation and droplet growth. The resulting governing equation systems are written as (7)

$$\frac{\partial Q}{\partial t}+\frac{\partial E}{\partial x}+\frac{\partial F}{\partial y}=\frac{1}{\mathrm{Re}}\left(\frac{\partial R}{\partial x}+\frac{\partial S}{\partial y}\right)+H \tag{1}$$

where

$$Q=\begin{bmatrix}\rho_m\\ \rho_m u\\ \rho_m v\\ \rho_m E_t\\ \rho_m g\\ \rho_m D_1\\ \rho_m D_2\\ \rho_m D_3\end{bmatrix},E=\begin{bmatrix}\rho_m u\\ \rho_m u^2+p\\ \rho_m uv\\ u(\mathrm{E_t}+p)\\ \rho_m ug\\ \rho_m uD_1\\ \rho_m uD_2\\ \rho_m uD_3\end{bmatrix},F=\begin{bmatrix}\rho_m v\\ \rho_m v\\ \rho_m v^2+p\\ v(E_t+p)\\ \rho_m vg\\ \rho_m vD_1\\ \rho_m vD_2\\ \rho_m vD_3\end{bmatrix}$$

$$R=\begin{bmatrix}0\\ \tau_{xx}\\ \tau_{xy}\\ \alpha\\ 0\\ 0\\ 0\\ 0\end{bmatrix},S=\begin{bmatrix}0\\ \tau_{yx}\\ \tau_{yy}\\ \beta\\ 0\\ 0\\ 0\\ 0\end{bmatrix},H=\begin{bmatrix}0\\ 0\\ 0\\ 0\\ \rho_m\dot{g}\\ \rho_m\dot{D}_1\\ \rho_m\dot{D}_2\\ \rho_m\dot{D}_3\end{bmatrix} \tag{2}$$

In these equations,

$$E_t=\rho_m C_{p0}T-p+\frac{1}{2}\rho_m(u^2+v^2)-\rho_m gL \tag{3}$$

$$\alpha=u\tau_{xx}+v\tau_{yx}+\frac{\mu}{(\gamma-1)\,\mathrm{Pr}}\frac{\partial T}{\partial x} \tag{4}$$

$$\beta=u\tau_{xy}+v\tau_{yy}+\frac{\mu}{(\gamma-1)\,\mathrm{Pr}}\frac{\partial T}{\partial y} \tag{5}$$

$$p=G\left[E_t-\frac{1}{2}\rho_m(u^2+v^2)+\rho_m gL\right] \tag{6}$$

$$G=\left(1-g\frac{M_m}{M_v}\right)\Big/\left(\frac{1}{\gamma-1}+g\frac{M_m}{M_v}\right) \tag{7}$$

$$L=3105913.39-2212.97\times10^{-2}\times T(J/kg) \tag{8}$$

τ_{xx}, τ_{xy}, τ_{yx} and τ_{xx}, as noted above, are components of viscous shear stresses. The value $g\left(\equiv\frac{m_l}{m_a+m_v+m_l}\right)$ denotes condensate mass fraction. The subscript m refers to the mixture. g, D_1, D_2, D_3 are given as follows:

$$\dot{g}=\frac{dg}{dt}=\frac{\rho_l}{\rho_m}\frac{4\pi}{3}\left(r_c^{\,3}I+\rho_m D_1\frac{\partial r}{\partial t}\right) \tag{9}$$

$$\dot{D}_1=\frac{dD_1}{dt}=\frac{4\pi r_c^{\,2}I}{\rho_m}+D_2\frac{dr}{dt} \tag{10}$$

$$\dot{D}_2=\frac{dD_2}{dt}=\frac{8\pi r_c^{\,2}I}{\rho_m}+D_3\frac{dr}{dt} \tag{11}$$

$$\dot{D}_3=\frac{dD_3}{dt}=\frac{8\pi I}{\rho_m} \tag{12}$$

The rate of formation of condensation droplet embryos per unit mass of mixture I (Frenkel's equation), the saturation pressure of droplet $p_{s,r}$, the critical radius of the condensation nuclei r_c, and the radius growth rate $\dot{r}$ are obtained from the classical theories of homogeneous condensation as follows:

$$I=\frac{1}{\rho_l}\left(\frac{p_v}{kT}\right)^2\sqrt{\frac{2\sigma M_v}{N_A\pi}}\exp\left\{\frac{-4\pi\sigma r_c^{\,2}}{3kT}\right\} \tag{13}$$

$$p_{s,r}=p_{s,\infty}\exp\left(\frac{2\sigma_\infty}{\rho_l R_v T_v}\right) \tag{14}$$

$$r_c=\frac{2\sigma}{\rho_l\Re T\ln\left(p_l/p_\infty\right)} \tag{15}$$

$$\dot{r}=\frac{dr}{dt}=\frac{\zeta_c}{\rho_l}\frac{p_\infty}{\sqrt{2\pi\Re T}}\left(\frac{p_v}{p_\infty}-1\right) \tag{16}$$

In Eq. (14), the flat film saturation pressure $p_{s,\infty}$ is given as [12]:

$$p_{s,\infty}(T)=\exp(A_1+A_2T+A_3T^2+A_4\ln(T)+\frac{A_5}{T})(atm) \tag{17}$$

Here, A_1=21.215, A_2=-2.7246*10^{-2}, A_3=1.6853*10^{-5}, A_4=2.4576, and A_5=-6094.4642, respectively.

With regard to the equations above, M, $\Re$, k, and p_∞ represent molecular weight, gas constant, Boltzman constant, and flat-film equilibrium vapor pressure, respectively. Subscripts v and l refer to the vapor and liquid phases, respectively. With regard to Eq.(16), ξ_c is a condensation coefficient. The surface tension for droplet σ is given by using the surface tension of an infinite flat-film σ_∞ and the surface tension coefficient ζ [12]

$$\sigma=\zeta\sigma_\infty \tag{18}$$

$$\sigma_{\infty}(T)=\begin{Bmatrix}\left[76.1+0.155\times(273.15-T)\right]\times10^{-3}\\(N/m)(T\geq249.39K)\\\left[(1.1313-3.7091\times10^{-3}\times T)\right]\times10^{-6}\\\times10^{-4}-5.6464\\(N/m)(T\langle249.39K)\end{Bmatrix} \quad (19)$$

(N/m)

In the computation, the values chosen for ξ_c and ζ are assumed to be 0.1 and 1.0, respectively [13]. The Baldwin-Lomax model [14] is utilized to solve the turbulence stresses. A third-order TVD finite difference scheme with MUSCL [15] is used to discretize the spatial derivatives of the governing equations, and a second-order central difference scheme is applied to the viscous terms. A second-order fractional time step is employed with regard to time integration.

4. Results and discussions

In the present study, the MLNs of 1.4 in the exit design Mach number are first designed by using the methodology suggested by Hodge et al., which is based on the characteristic method. Next, the design validity can be verified by means of agreements between the numerical analysis results and the measurements in static pressure normalized with stagnation pressure along the nozzle centerline for (T_0=290K, p_0=101.3 kPa and ϕ_0=30%) and of 1.4 in the nozzle exit Mach number by numerical analysis for (T_0=290K, p_0=101.3 kPa and ϕ_0=0%); here, the stagnation relative humidity ϕ_0 is defined as p_{V0}/p_{S0}. Both results are shown in Fig. 2. Here, h represents the throat height of the nozzle, and x=0 corresponds to the position of the nozzle throat. As shown in the figure, the distributions of static pressure based on the results of numerical analysis and measurement along the nozzle centerline are synonymous; however, the distribution of the Mach number at the nozzle exit plane slightly differs from the value of 1.4 in the nozzle design Mach number, which is caused by the fact that we did not take into account the viscous effect with regard to the method of characteristics. Owing to the effect of the initial expansion fan centered at the sharp corner of the nozzle throat, as shown in the iso-Mach number plot, the increasing rate with regard to the Mach number at the vicinity of the wall is larger than that around the nozzle centerline. As a whole, it can be concluded that the nozzle is properly designed. The distributions of static pressure and the Mach

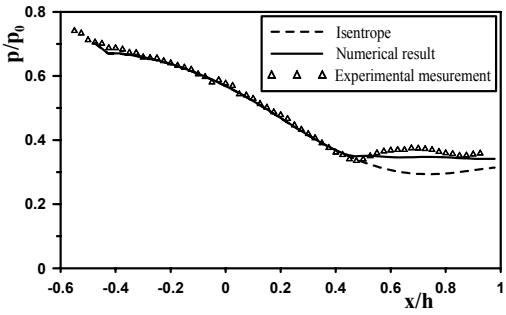

(a) Static pressure distribution (ϕ_0= 30%)

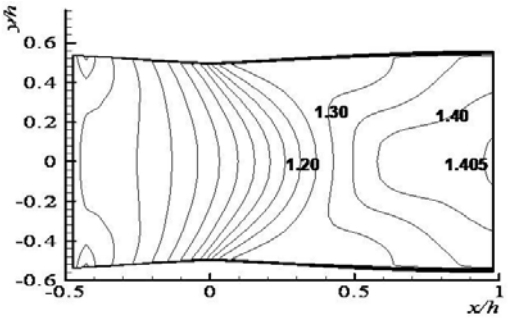

(b) Iso-Mach number plot(ϕ_0= 0%)

Fig. 2. Static pressure distribution along the nozzle centerline and iso-Mach number plot (T_0=290K and p_0=101.3 kPa).

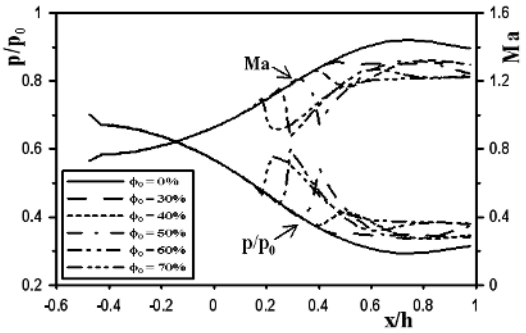

Fig. 3. Distributions of flow property along the nozzle centerline with ϕ_0 (p_0=101.3 kPa and T_0=290K).

number along the nozzle centerline with ϕ_0 are shown in Fig. 3. In general, the higher ϕ_0 is, the larger the condensable mass fraction for the same T_0 becomes; the onset point of nonequilibrium condensation corresponding to the deviation point from the isentrope moves upstream with the increase of ϕ_0. The degree of deviation from the isentrope (that is, ϕ_0=0% in this case) increases with the increase in ϕ_0. In special, in spite of smallness of ϕ_0, it turns out that the deceleration of flow by heat addition and its gradient for

ϕ_0=60% are larger than those for ϕ_0=70%. These are caused by the fact that the onset point of nonequilibrium condensation at the nozzle centerline for ϕ_0=70% lies at the incident region ahead of the expansion waves emanating from the sharp corner just downstream of the nozzle throat. Fig. 4 shows the schlieren photographs and iso-pressure plots, with variations of ϕ_0 for the design exit Mach number of 1.4 and T_0=290K, respectively. As shown in the photograph and iso-pressure plot for ϕ_0=30%, we could not find any flow disturbance caused by the influence of nonequilibrium condensation. However, in cases with a condensation shock wave (b-d) caused by the increase in released latent heat by nonequilibrium condensation to the surroundings, it can be determined that the position of the condensation shock wave moves upstream with the increase in ϕ_0. Owing to the nature of two-dimensional MLNs, we can see that the onset of nonequilibrium condensation at the upper wall is faster in comparison to the nozzle centerline. In flows with a condensation shock wave, the

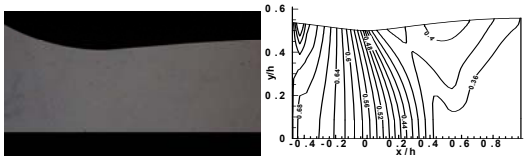

(a) ϕ_0=30%

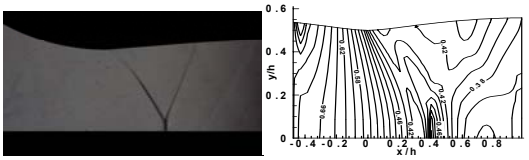

(b) ϕ_0=50%

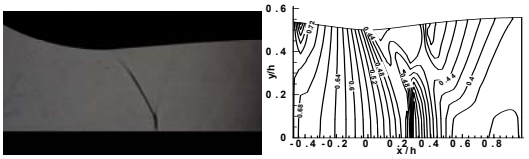

(c) ϕ_0=60%

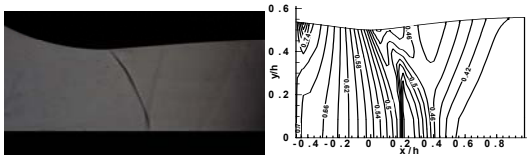

(d) ϕ_0=70%

Fig. 4. Schlieren photographs and iso-pressure plots with ϕ_0.

X-type condensation shock wave changes to λ type with the increase in stagnation relative humidity. Also, the larger the stagnation relative humidity is, the longer the length of the normal portion of the condensation shock wave becomes. In Fig. 5, the liquid mass fraction g with ϕ_0 along the nozzle centerline is plotted, and we can see that the final liquid mass fraction g becomes larger with the increase in ϕ_0, and the onset point of nonequilibrium condensation moves upstream with the increase in ϕ_0. We can also see that the condensable water vapor of the mixture nearly condenses into liquid through the process of nonequilibrium condensation, which is assessed from the flattened gradient in g. For example, the condensate liquid mass fraction g in the case of (p_0=101.3 kPa, T_0=290K and ϕ_0=70%) approaches the final value of 0.0075, in which the specific humidity at the stagnation point ω_0 is 0.0079. The distributions of the degree of supersaturation along the nozzle centerline with ϕ_0 are shown in Fig. 6. As expected, because of the eases of condensation onset for a large ϕ_0, the condensation onset point moves upstream, and the degree of supersaturation at the onset of condensation becomes smaller with the increase in ϕ_0. The momentum efflux per unit nozzle width from the nozzle exit relates directly to the thrust of the nozzle system as shown in Fig. 7. The momentum efflux from the nozzle can be calculated as the Momentum efflux = $\int_0^{y_e} 2\rho v^2 dy$ as noted, y_e and v refer to half the height of the nozzle exit and exit velocity ($v = \sqrt{kRTM}$), respectively. This may be summarized as follows: the larger the stagnation humidity for the same T_0, p_0, and nozzle geometry, the lesser the efflux momentum becomes.

This is caused by the fact that the larger the specific humidity is, the larger the release of latent heat by the condensation into the surrounding supersonic gas

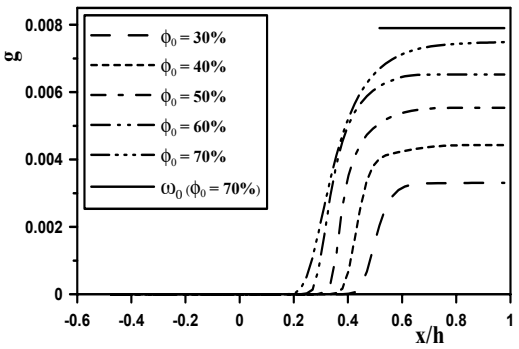

Fig. 5. Distributions of the liquid mass fraction g with ϕ_0.

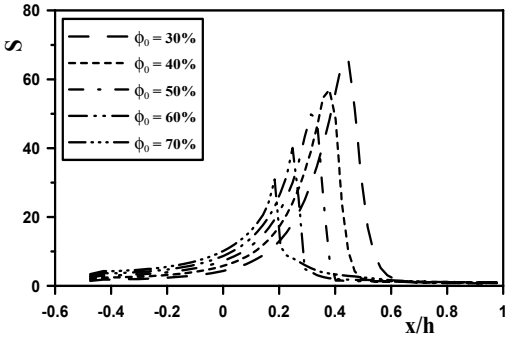

Fig. 6. Distributions of the degree of supersaturation along the nozzle centerline with ϕ_0.

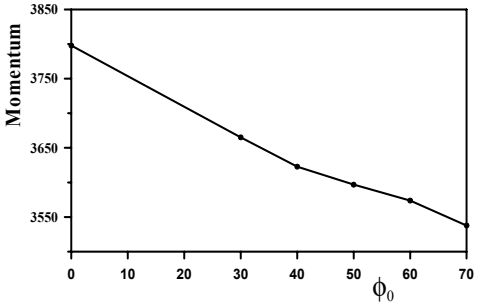

Fig. 7. Momentum efflux with ϕ_0 (T_0=290K, p_0=101.3 kPa and M_a=1.4).

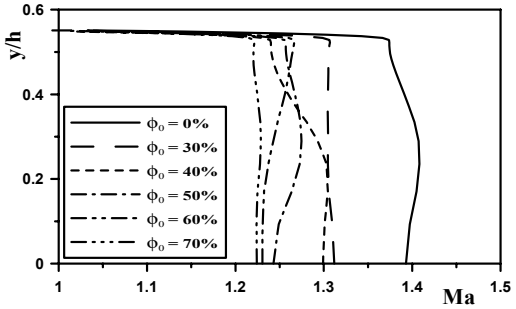

(a) Mach number

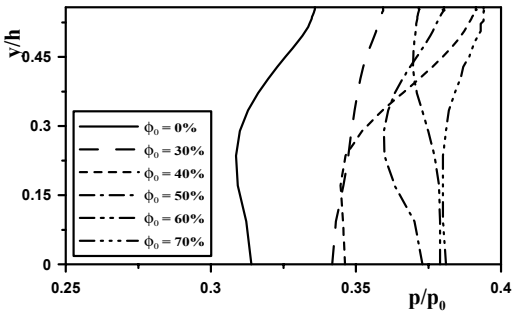

(b) Static pressure

Fig. 8. Distributions of Mach number and static pressure at the nozzle exit with ϕ_0(T_0=290K, p_0=101.3 kPa and M_a=1.4).

flow, which results in the larger deceleration of the surrounding supersonic flow. The momentum decreases linearly with the increase in ϕ_0 on a percentage basis.

Finally, distortions from the isentropic flow (that is, the case of ϕ_0=0%) in the nozzle exit Mach number, as well as the static pressure with ϕ_0, are shown in Fig. 8. Because of the addition of the latent heat released by the nonequilibrium condensation process to the surrounding supersonic flow, we can see that the distortion from the isentrope increases with the increase in ϕ_0. Owing to the fact that we did not take into account the viscous effect in the design of MLNs, the Mach number and static pressure for ϕ_0=0% at the nozzle exit plane differ somewhat from the design values.

5. Conclusions

Based on the flow of moist air through a nearly minimum length nozzle, which was designed by the method of characteristics, the effects of nonequilibrium condensation on the uniformity of flow properties at the nozzle exit, the momentum, and the flow distortion at the nozzle exit plane are presented by experiment and numerical analysis. The obtained results are summarized as follows:

(1) The uniformity of flow properties at the nozzle exit for the flow with nonequilibrium condensation in the minimum length nozzle cannot be guaranteed.

(2) The decrease in momentum efflux, which is based on the nozzle exit for the stagnation relative humidity of ϕ_0=70% (T_0=290K), is 6.8% smaller than that of the isentropic expansion process.

(3) The distortions which deviated from the isentrope at the nozzle exit plane become larger with the increase in ϕ_0.

Acknowledgment

The authors are grateful to Professors Setoguchi T. and Matsuo S. of Saga University in Japan for their valuable help in providing numerical calculations.

Nomenclature

C_p : Constant pressure specific heat [J/(kg · K)]
D_1, D_2, D_3 : Dummy variables
E_t : Total energy per unit volume [J/m^3]
E, F : Numerical flux

f : Frequency [kHz]
g : Liquid mass fraction
h : Throat height [mm]
H : Source term
I : Nucleation rate [l/(m^3 · s)]
k : Boltzmann constant [J/K]
L : Latent heat [J/kg]
m : Mass [kg] or molecular weight [kg/kmol]
Pr : Prandtl number
p : Static pressure [Pa]
p_∞ : Flat film equilibrium vapor pressure [Pa]
Q : Conservation mass term
R, S : Viscous term
r : Droplet radius [m]
r_c : Critical droplet radius [m]
S : Degree of supersaturation
t : Time [s]
T : Temperature [K]
u, v : Cartesian velocity components [m/s]
x, y : Cartesian Coordinate
ϕ : Relative humidity ($\equiv p_V/p_S$)
γ : Specific heat ratio
μ : Dynamic viscosity [Pa · s]
ζ : Coefficient of surface tension
σ : Surface tension [N/m]
ρ : Density [kg/m^3]
$\Re$: Gas constant [J/(kg · K)]

subscripts

0 : Stagnation condition
l : Liquid
m : Mixture
r : Droplet radius
v : Vapor
∞ : Infinite plane surface

References

[1] P. P. Wegener, Nonequilibrium flow with condensation, *Acta Mechanica*, 21 (1-2) (1975) 65.

[2] R. A. Oriani and B. E. Lundquist, Emendations to Nucleation Theory and the Homogeneous Nucleation of Water from the Vapour, *J.Chem.Phys*., 38 (1963) 2082.

[3] J. Lothe and G. M. Pound, *In Nucleation*, edited by Zettlemoyer, A. C. Marcel Dekker, New York, (1969) chpt. 3.

[4] J. P. Sislian and I. I. Glass, Condensation of Water Vapour in Rarefaction Waves: I. Homogeneous Nucleation, Dec., *AIAA, J.*, 14 (12) (1976) 1731-1737.

[5] S. C. Baek, S. B. Kwon, H. D. Kim, T. Setoguchi and S. Matsuo, Study of Moderately Underexpanded Supersonic Moist Air Jets, *AIAA, J.*, 44 (7) (2006) 1624-1627.

[6] S. B. Kwon and H. J. Ahn, Supersonic Moist Air Flow with Condensation in a Wavy Wall Channel, *KSME*, *Int.J.*, 15 (4) (2001) 492-499.

[7] S. C. Baek, S. B. Kwon and H. D. Kim, Passive Prandtl-Meyer Expansion Flow with Homogeneous Condensation, *KSME,Int.J.*, 18 (3) (2004) 407-418.

[8] M. Stastny and M. Sejna, Numerical Simulation of the Steam Flow with Condensation in a Nozzle, *14th Int. Conf. on the Properties of Water Steam in Kyoto*, (2004) 637-642.

[9] J. D. Anderson Jr., *Gas dynamic Lasers: An Introduction*, Academic, New York (1976).

[10] B. K. Hodge and K. Koenig, *Compressible Fluid Dynamics with Personal Computer Applications*, Prentice Hall, Upper Saddle River, NJ. (1995) 466-477.

[11] H. Y. Wachman, The Thermal Accommodation Coefficient: A Critical Survey, *ARS J*, 32 (9) (1962) 2-12.

[12] U. Dohrmann, *Ein Numerisches Verfahren zur Berechnung stationarer transsonischer Stromungen mit Energiezufuhr durch homogene Kondensation*, doctors der Ingenieurwissenschaften, Uni. Karlsruhe (1989).

[13] S. Adam and G. Schnerr, Instabilities and Bifurcation of Nonequilibrium Two-phase Flows, *Journal of Fluid Mechanics*, 348 (1997) 1-28.

[14] B. S. Baldwin and H. Lomax, Thin Layer Approximation and Algebraic Model for Separated Turbulent Flows, *AIAA*, 257 (1978) 9.

[15] H. C. Yee, A Class of High Resolution Explicit and Implicit Shock-capturing Methods, *NASA, TM-89464* (1989).

Soon-Bum Kwon received his B.S. and M.S. degrees in Mechanical Engineering from Kyungpook National University in 1974 and 1980, respectively, and his Ph.D. degree from Kyushu University in 1987. He is a Professor at the School of Mechanical Engineering at Kyungpook National University. His research interests are compressible gas dynamics and nonequilibrium condensation.